HEFAT2012
9th International Conference on Heat Transfer, Fluid Mechanics and Thermodynamics
16-18 July 2012
Malta

NUMERICAL ANALYSIS OF THERMAL PERFORMANCE OF AN EXTERNALLY LONGITUDINALLY FINNED RECEIVER FOR PARABOLIC TROUGH SOLAR COLLECTOR

Mwesigye A., Bello-Ochende T.* and Meyer J. P.
*Author for Correspondence
Department of Mechanical and Aeronautical Engineering
University of Pretoria
Pretoria 0002
South Africa
*Email: tbochende@up.ac.za

ABSTRACT
A receiver is a central component of the parabolic trough collector system. Its design and state greatly affects performance of the entire collector system. In this paper a three dimensional numerical model of a receiver with an externally longitudinally finned absorber tube was developed to study the effect of fin dimensions on heat transfer and fluid flow performance characteristics. Results show that external longitudinal fins improve the performance of the receiver. Results further show that collector efficiency and useful heat gain will increase as the fin thickness and height increase and so do heat losses, glass temperature and maximum absorber temperature. A 6% increase in efficiency and a pressure drop of 370.65Pa/m are obtained for a finned absorber tube with lower dimensions 1.0 cm x 0.2 cm when compared to a non-finned tube larger in diameter by 1 cm. An increase in efficiency of 8% is obtained when the same finned absorber tube is compared with a non-finned tube of the same size.

INTRODUCTION
The increasing concerns of climate change and global warming driven by emission of large amounts greenhouse gasses into the atmosphere mainly from utilization of fossil based energy resources, together with the increasing demand for energy has led to increased search for efficient and clean alternative energy sources and technologies [1]. In order to make alternative renewable energy technologies acceptable they must be efficient, reliable, cost effective and producing electricity at prices competitive with that from conventional resources.

Of the alternative energy resources, solar energy is the world's most abundant and clean source of energy. It has an enormous potential for supplying a significant portion of the world's energy demand [2, 3] and presents an opportunity for distributed energy generation as well as meeting the energy needs of majority rural populations currently without access to modern energy services since it is widely available. But significant research is still needed to harness this resource efficiently, at competitive prices and making it reliable.

Concentrated Solar Power (CSP) has gained acceptance for solar thermal electricity generation with parabolic trough collectors the most commercially and technically developed. The construction and successful operation of the first plants, the Luz Solar Electricity Generating Systems commonly known as SEGS in California's Majove Desert was a major breakthrough of parabolic trough collector technology [2, 4, and 5]. With an installed capacity of about 354MW, the plants have been in operation since early 1980's. They operate with heat transfer fluid temperatures between 293^{o}C – 391^{o}C. With recent technology advances the cost of electricity from PTCs is said to be approaching that of small-medium sized coal power plants and further cost reductions are possible with improved receiver designs, increased concentrator sizes, and improved thermal storage systems [6, 7].

However, despite successful operation of the SEGS plants there are still challenges to the operation of parabolic trough collector systems which include; increased heat losses at higher absorber temperatures, vacuum loss, degradation of the selective coating, glass breakages attributed to the high temperature gradients along the absorber tube circumference and concentrated heat flux hitting the glass to metal seal [4]. Therefore, research is still needed to address these challenges and improve collector performance.

A number of studies have been carried out to investigate parabolic trough collector system performance ranging from studies on entire system performance [8, 9, 10, 11 and 12] to studies on only the receiver. Dudley [11, 12] carried out tests on SEGS LS-2 and Industrial Solar Technology (IST) solar collectors respectively with different coatings and different configurations in the annulus space. Receivers with vacuum in annulus space had superior performance over those without. Odeh and Morrison [13] studied the dependence of thermal losses on air velocity. Liu et al. [14] developed an experimental platform for investigating parabolic trough solar collector performance. Experiments showed that collector efficiency increases with volume flow rate. Measured efficiencies were in the range 40 – 60% and heat losses about 220W/m when the temperature difference between absorber and ambient was 180^{o}C.

Studies have also been carried out on receiver heat loss determination and receiver performance monitoring. Prince et al. [15] used a solar blind Infrared camera to monitor over 12,000 receivers at the SEGS plants. Glass temperatures between 30 – 170^{o}C were obtained depending on: the type of

receiver, time in operation and whether the receiver has hydrogen removers or not. The cermet coated receiver with hydrogen removers showed good results with glass temperature between 50° and 100°C no matter the age and some less than 50°C. Lupfert et al. [16] also used a solar blind infrared camera to measure temperature along the absorber circumference and compared results with those from ray trace methods. The temperature along the tube circumference was found to vary along tube circumference but was uniform along the length of the absorber. Lupfert et al. [17], Burkholder and Kutscher [18, 19] used laboratory steady state tests to measure receiver heat losses. Receiver losses were found to depend on incident radiation and absorber temperature. For the Solel UVAC3 the receiver losses were in the range 15–460W/m depending on absorber temperature and ambient temperature [18]. Forristall [20] developed a heat transfer model for determining the performance of parabolic trough receiver implemented in Engineering Equation Solver (EES). The performance was derived from energy balances between collector, receiver and air. The model was in agreement with experimental results obtained by Dudley [11].

To take into account the differential heat flux on the absorber tube surface, He et al. [21] used Monte-Carlo ray trace methods and a finite volume method to study flow and heat transfer characteristics of the working fluid inside the absorber.

Performance enhancement of receivers has received considerable attention in the last two decades. Hegazy [22] analytically considered possible use of external longitudinal fins on an absorber tube and found that the efficiency of the collector can be increased by 2.5 – 4.5 %. Reddy et al. [23] used numerical methods to perform thermal analysis on a receiver with porous and longitudinal internal fins. The study shows a heat transfer enhancement of 21% with a porous fin when compared to a longitudinal fin. Kumar and Reddy [24] extended the analysis done by Reddy et al. [23] to a receiver with a porous disc oriented at different angles to the absorber axis. A 64.2% increase in Nusselt number was achievable but with a pressure drop penalty of 457Pa. Munoz and Abanades [25] investigated an internally helically finned absorber tube with a view of evening out the non-uniform absorber circumferential temperatures. From the study a 3% increase in collector efficiency and 40% reduction in absorber temperature difference is achievable while the pressure drop increased by 10 - 50 % depending on the fin arrangement.

The purpose of this study is to numerically investigate the performance of an externally longitudinally finned absorber tube of a parabolic trough receiver. Variation of receiver efficiency, receiver heat losses, absorber maximum temperature; pressure drop and glass temperature with fin dimensions are investigated. It is assumed that the lower fin and lower half of the absorber receive the same concentrated heat flux.

PHYSICAL MODEL AND GOVERNING EQUATIONS

The parabolic tough solar collector is simply made by bending a sheet of metal into a parabolic shape with a receiver along its focal axis as shown in Figure 1. The receiver consists of a steel absorber tube enclosed in a glass jacket that is evacuated to reduce convection heat losses; the glass and tube are sealed with glass to metal seals and provided with getter material as shown in Figure 2 to absorb any hydrogen that infiltrates from the heat transfer fluid. Reflected solar energy is incident on the lower half of the absorber tube as in Figure 3 where most of it is absorbed and conducted through the absorber tube wall and carried by the heat transfer fluid to the heat exchangers of the power block while the rest is radiated and conducted to the glass envelope and lost to the environment.

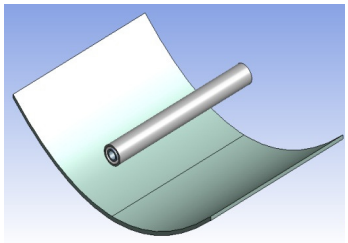

Figure 1 Parabolic trough collector

Therefore, heat transfer in the receiver consists of forced convection inside the absorber tube, conduction within the absorber walls and radiation in the glass envelope when fully evacuated. Combined radiation and free molecular conduction will occur in the glass envelop when not fully evacuated or combined radiation and natural convection when the glass envelop is broken or non-existent.

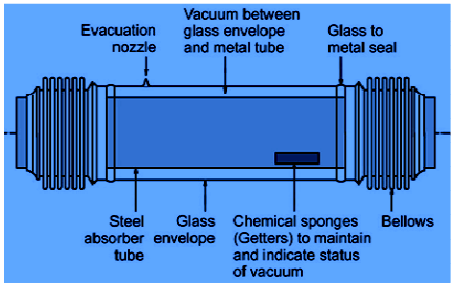

Figure 2 Evacuated receiver tube

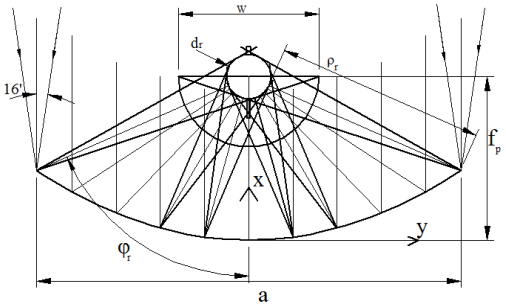

Figure 3 Ray trace diagram for a parabolic trough collector

The proposed model of the receiver consists of fins that are external to the absorber tube as shown in Figure 4. With this arrangement the absorber diameter can be kept small, larger receiver aperture widths can be used, thus higher concentration ratios. Moreover, an almost uniform heat flux on the lower half of the absorber tube can be achieved. Further still, since the receiver's annulus is evacuated and absorber surface is usually coated with a selective coating, natural convection is suppressed and radiation losses are minimised. As a result most

of the incident solar radiation on the fin must be conducted to the absorber tube improving performance.

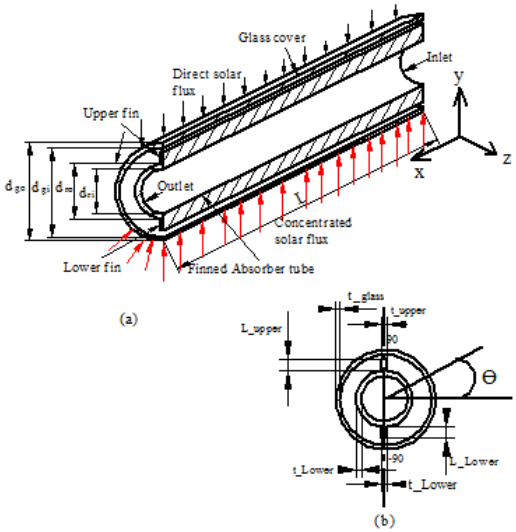

Figure 4 (a) Computational domain (b). Finned receiver cross-section

The diameter of the absorber to intercept the entire solar image derived from ray trace diagram in Figure 3 is given equation (1) [26] for a trough of perfect alignment and shape and considering sun's shape as perfect.

$$d_r = 2\rho_r \sin 0.267 = \frac{a \sin 0.267}{\sin \varphi_r} \tag{1}$$

Whereas the size of the flat receiver or the diameter of the semi-circular receiver to intercept the entire solar image is given by equation (2) [26] also derived from Figure 3

$$W = \frac{2\rho_r \sin 0.267}{\cos(\varphi_r + 0.267)} = \frac{a \sin 0.267}{\sin \varphi_r \cos(\varphi_r + 0.267)} \tag{2}$$

Since d_r is usually very small absorber diameters between d_r and W are commonly used mainly to avoid higher local concentration of solar radiation on tube surface [21]. Therefore, combining a small absorber diameter with external fins would alleviate such hot spots.

The performance of the parabolic trough collector is quantitatively expressed in terms of the heat gained by the working fluid and collector efficiency given by equations (3) and (4) respectively.

$$q_u = I_b \eta_o A_a - Q_{loss} = \dot{m}_f c_p (T_{out} - T_{in}) \tag{3}$$

Collector efficiency is given by

$$\eta = \frac{q_u}{I_b A_a} \tag{4}$$

Heat transfer in the annulus space

In the annulus receivers are manufactured with a high vacuum (P < 0.013Pa) [11, 27] in order to activate the getters that absorb hydrogen released by the heat transfer fluid and then diffusing through the absorber into the vacuum jacket. In this highly evacuated gap the heat transfer is only by radiation. At moderate vacuum pressures heat loss is by both radiation and molecular conduction since the gas density will be too low to support free convection. For very low pressures the behaviour of air depends on the mean free path, χ (m) of the gas molecules defined by equation (5) [27] as

$$\chi = \frac{\mu}{P}\sqrt{2R_s T} \tag{5}$$

As the pressure in the annulus reduces the mean free path of the air molecules becomes larger and the assumption of a continuum model breaks down for convection heat transfer modelling. As such the mean free path needed to maintain the continuum model in the receiver's annulus is calculated to be above 30 Pa. Heat loss for a collector of length (L) is given by equations (6) and (7) [2, 26]. Heat lost by the absorber tube is the same as the heat lost to the surrounding environment.

$$Q_{loss} = \frac{2\pi\lambda_{eff}}{\ln \frac{d_{gi}}{d_{ro}}}(T_{ro} - T_{gi}) + \frac{\pi d_{ro} L \Phi (T_{ro}^{\ 4} - T_{gi}^{\ 4})}{\frac{1}{\xi_{ro}} + \frac{1-\xi_{gi}}{\xi_{gi}}\left(\frac{d_{ro}}{d_{gi}}\right)} \tag{6}$$

$$Q_{loss} = \pi d_{go} L h_w (T_{go} - T_{amb}) + \xi_g \pi d_{go} L \Phi (T_{go}^{\ 4} - T_{sky}^{\ 4}) \tag{7}$$

Where $\lambda_{eff,air}$ is the effective conductivity between the glass cover and the receiver system given by equation (8) as given by [26]

$$\frac{\lambda_{eff,air}}{\lambda_{air}} = \max\left[1,\ 0.386\left(\frac{\Pr \times Ra^*}{0.861 + \Pr}\right)^{\frac{1}{4}}\right] \tag{8}$$

Where

$$Ra^* = \frac{\left(\ln {d_{ro}}/{d_{ri}}\right)^4}{L^3\left(d_{ri}^{-3/5} + d_{ro}^{-3/5}\right)^5} Ra \tag{9}$$

And

$$Ra_L = \frac{g\beta(T_{ro} - T_{gi})L^3 \Pr}{v^2} \tag{10}$$

For very low vacuum pressures $\lambda_{eff,air}$ approaches zero and only radiation heat transfer should be considered. Air thermal conductivity for low pressures has been determined from equation (11) [28]

$$\lambda_{air} = \lambda_{air,o} \frac{1}{1 + \frac{7.6x10^{-5}}{P\,{d_{rg}}/{T}}} \tag{11}$$

Where d_{rg} is the glass cover-absorber tube spacing

The sky temperature has been calculated from the relation by [29]

$$T_{sky} = 0.0552 T_{amb}^{1.5} \tag{12}$$

While the emissivity of glass is given as $\xi_{gi} = 0.86$ [18, 20] and the absorber emissivity varies with wall temperature. For cerment selective coating is absorber emissivity is given by [20] as

$$\xi_{ro} = 0.0003 1 T_{ro} - 0.0216 \tag{13}$$

The average wind heat transfer coefficient h_w was estimated using the expression given by [19] as

$$h_w = 4.9 + 4.9 v_w - 0.18 v_w^2 \tag{14}$$

Thermal analysis of flow and heat transfer inside the absorber tube

Determination of Reynolds numbers for flow in the absorber tube for velocities above 0.25m/s indicates that the flow is turbulent. Therefore, Reynolds Averaged Navier Stokes (RANS) equations are used to model heat transfer and flow in the absorber tube. For steady state, incompressible, turbulent, axisymmetric flow the RANS equations for continuity, momentum and energy are given by equations (15 – 18) [30, 31].

Continuity equation

$$\frac{\partial \rho \bar{u}}{\partial x} + \frac{1}{r}\frac{\partial}{\partial r}(\rho r \bar{v}) = 0 \tag{15}$$

Axial momentum

$$\rho\left[\bar{u}\frac{\partial \bar{u}}{\partial x} + \bar{v}\frac{\partial \bar{u}}{\partial r}\right] = -\frac{d\bar{P}}{dx} + \frac{\partial}{\partial x}\left(\mu_{eff}\frac{\partial \bar{u}}{\partial x}\right) + \frac{1}{r}\frac{\partial}{\partial r}\left(\mu_{eff}\frac{\partial \bar{u}}{\partial r}\right) + \left[\frac{\partial}{\partial x}\left(\mu_{eff}\frac{\partial \bar{u}}{\partial x}\right) + \frac{1}{r}\frac{\partial}{\partial r}\left(r\mu_{eff}\frac{\partial \bar{v}}{\partial x}\right)\right] \tag{16}$$

Radial component

$$\rho\left[\bar{v}\frac{\partial \bar{v}}{\partial r} + \bar{u}\frac{\partial \bar{v}}{\partial x}\right] = -\frac{\partial \bar{p}}{\partial r} + \frac{\partial}{\partial x}\left(\mu_{eff}\frac{\partial \bar{v}}{\partial x}\right) + \frac{1}{r}\frac{\partial}{\partial r}\left(r\mu_{eff}\frac{\partial \bar{v}}{\partial r}\right) + \left[\frac{\partial}{\partial x}\left(\mu_{eff}\frac{\partial \bar{u}}{\partial r}\right) + \frac{1}{r}\frac{\partial}{\partial r}\left(r\mu_{eff}\frac{\partial \bar{v}}{\partial r}\right)\right] - 2\mu_{eff}\frac{\bar{v}}{r^2} \tag{17}$$

The Energy equation assuming no viscous heating by the heat transfer fluid is given by

$$\rho c_p\left[\bar{u}\frac{\partial \bar{T}}{\partial x} + \bar{v}\frac{\partial \bar{T}}{\partial r}\right] = \frac{\partial}{\partial x}\left(\lambda_{eff}\frac{\partial \bar{T}}{\partial x}\right) + \frac{1}{r}\frac{\partial}{\partial r}\left(r\lambda_{eff}\frac{\partial \bar{T}}{\partial r}\right) \tag{18}$$

Where

$$\mu_{eff} = \mu_t + \mu$$

λ_{eff} is the effective fluid thermal conductivity and for the standard k-ε and realizable model is given by [31] as

$$\lambda_{eff} = \lambda + \frac{c_p \mu_t}{\mathrm{Pr}_t} \tag{19}$$

Because RANS equations present a closure problem additional equations are needed to obtain all the unknowns. Turbulence modelling is usually used to remedy such a problem. Of the available turbulent models the k-ε model and its improvements of k-ε RNG (Renormalization group) and the k-ε Realizable models are the most widely used and validated models for most flows [32]. The RNG and Realizable k-ε models are improvements of the standard k-ε model. In this study the Realizable k-ε model was used. The k-ε models have two equations for the turbulent energy (k) and dissipation rate (ε).

The transport equations for the Realizable k-ε model are given by equations (20 -23) [31];

k- Equation

$$\rho\left[\bar{u}\frac{\partial k}{\partial x} + \bar{v}\frac{\partial k}{\partial r}\right] = \frac{\partial}{\partial x}\left[\left(\mu + \frac{\mu_t}{\sigma_k}\right)\frac{\partial k}{\partial x}\right] + \frac{1}{r}\frac{\partial}{\partial r}\left[r\left(\mu + \frac{\mu_t}{\sigma_k}\right)\frac{\partial k}{\partial r}\right] + G - \rho\varepsilon \tag{20}$$

ε- Equation

$$\rho\left[\bar{u}\frac{\partial \varepsilon}{\partial x} + \bar{v}\frac{\partial \varepsilon}{\partial r}\right] = \frac{\partial}{\partial x}\left[\left(\mu + \frac{\mu_t}{\sigma_\varepsilon}\right)\frac{\partial \varepsilon}{\partial x}\right] + \frac{1}{r}\frac{\partial}{\partial r}\left[r\left(\mu + \frac{\mu_t}{\sigma_\varepsilon}\right)\frac{\partial \varepsilon}{\partial r}\right] + \rho C_{\varepsilon 1} S\varepsilon - C_{\varepsilon 2}\rho\frac{\varepsilon^2}{k + \sqrt{\nu\varepsilon}} \tag{21}$$

G, the generation of turbulent kinetic energy is given by

$$G = \mu_t S^2 = \mu_t\left[2\left\{\left(\frac{\partial \bar{v}}{\partial r}\right)^2 + \left(\frac{\partial \bar{u}}{\partial x}\right)^2 + \left(\frac{\bar{v}}{r}\right)^2\right\}\right] + \mu_t\left(\frac{\partial \bar{u}}{\partial r} + \frac{\partial \bar{v}}{\partial x}\right)^2 \tag{22}$$

σ_k is the turbulent Prandtl number for k, σ_ε is the turbulent Prandtl number for ε and G is the generation of turbulent kinetic energy due to the mean velocity gradients given as [31, 33]. The model constants are $C_{\varepsilon 2}$ = 1.9, σ_k = 1, σ_ε = 1.2. For Realizable k-ε model $C_{\varepsilon 1}$ is not constant and is determined as detailed in [31, 33]

Eddy viscosity calculation for the realizable model is given by

$$\mu_t = \rho C_\mu \frac{k^2}{\varepsilon} \tag{23}$$

C_μ is a function of the mean strain and rotation tensor whose detailed determination is given in [33]

Turbulent models do not resolve the flow characteristics in regions near walls since in these regions viscous forces are either equal in magnitude to inertia forces or larger. Near the wall velocity changes rapidly, solution gradients are very high, flow is influenced by the viscous effects and is independent of the parameters far from the wall. In ANSYS Fluent standard wall functions based on the works of Lauder and Spalding [33] and are widely used for most flows. The near wall node is modelled by laws of the wall [33]

The law of the wall for mean velocity yields

$$U^* = \frac{1}{\kappa}\ln(E\ y^*) \tag{24}$$

Where; κ is the Von Kàrmàn Constant = 0.4187and E is an empirical constant = 9.793

The dimensionless wall velocity U^* is given by

$$U^* \equiv \frac{U_p C_\mu^{1/4} k_p^{1/2}}{\tau_w / \rho} \tag{25}$$

And the dimensionless distance from the wall y^*

$$y^* \equiv \frac{\rho C_\mu^{1/4} k_p^{1/2} y_p}{\mu} \tag{26}$$

Where, k_p is the turbulent energy for the near wall node, y_p is the distance from the wall to near wall node and U_p is mean velocity for the near wall node.

The lower limit for use of wall functions is about y^* =15 and the upper limit depends strongly on the Reynolds number. Below the lower limit the accuracy of the solution cannot be maintained except when scalable wall functions are used. In this study scalable wall functions were used and they help when the grid is refined such that y^* <11 [33]. They force the usage

of the log-law in conjunction with standard wall functions approach.

Heat transfer and fluid flow inside the absorber tube can be characterized in terms of pressure drop and Nusselt number. The pressure drop along the absorber tube determines how much power must be used to force the fluid through the tube. Pressure drop (ΔP) is related to friction factor *f* by equation. (27).

$$\Delta P = f \frac{L}{D} \frac{\rho U^2}{2} \quad (27)$$

Where D is the hydraulic diameter given by the ration of area and wetted perimeter (p_w) as

$$D = \frac{4A}{p_w}$$

The required pumping power $\dot{W}_{pump}$ to overcome the pressure drop is given by

$$\dot{W}_{pump} = \dot{V} \Delta P \quad (28)$$

For smooth tubes the friction factor *f* is given by Petukhov first equation given in [34] put forward by Petukhov in 1970.

$$f = (0.790 \ln \mathrm{Re} - 1.64)^{-2} \quad (29)$$

Re is the dimensionless Reynolds number given by

$$\mathrm{Re} = \frac{\rho U D}{\mu}$$

The heat transfer is given in terms of the Nusselt Number (Nu) which is given as

$$Nu = \frac{hD}{k}$$

and the heat transfer coefficient h, is given as

$$h = \frac{q''}{T_w - T_{ref}} \quad (30)$$

For a constant heat flux along the absorber tube circumference, Nusselt number, Reynolds number and Prandtl number are correlated by the Gnielinski correlation given by equation (31) as was put forward by Gnielinski in 1976 [34] as an improvement of Petukhov's second equation [34] with all properties evaluated at bulk temperature.

$$Nu = \frac{\left(f/8\right)(\mathrm{Re} - 1000)\mathrm{Pr}}{1 + 12.7\left(f/8\right)^{0.5}\left(\mathrm{Pr}^{2/3} - 1\right)} \quad (31)$$

For $0.5 \le \mathrm{Pr} \le 2000$ and $3 \times 10^3 < \mathrm{Re} < 5 \times 10^6$

The boundary conditions used in the study for the annulus space and absorber tube are given as;

Receiver Annulus

At x = 0, $\frac{d_{ro}}{2} \le r \le \frac{d_{gi}}{2}$

u = v = 0

P_{in} = 40 bars

$T_{in} = T_{amb}$

Wall boundary conditions

A mixed convection and radiation boundary condition is used for glass cover outer surface.

At x = L, $\frac{d_{ro}}{2} \le r \le \frac{d_{gi}}{2}$

A zero pressure gradient at the annulus outlet is used

Absorber tube

At the inlet; x = 0, $0 \le r \le \frac{d_{ri}}{2}$, $-90^o \le \theta \le 90^o$

v = 0, $u = u_{in}$

$T = T_{in}$

Wall boundary conditions

At $r = \frac{d_{ri}}{2}$, $0 \le x \le L$, a no-slip boundary condition exists

On the outer surface of the absorber tube a uniform heat flux is assumed as in [23, 25] given as;

At $r = \frac{d_{ro}}{2}$, $0^o \le \theta \le 90^o$

$$q'' = \tau_g I_b$$

$r = \frac{d_{ro}}{2}$, $-90^o \le \theta \le 0^o$

$$q'' = \eta_0 C_R I_b \quad where \quad C_R = \frac{A_a}{A_r}$$

A_a is the aperture area projected on a horizontal plane and A_r is the corresponding absorber area, I_b is the direct solar radiation taken as 933W/m^2.

At the outlet (x = L, $0 \le r \le \frac{d_{ri}}{2}$) a zero pressure gradient is applied

On the symmetry plane, there is a zero normal velocity and zero normal gradients of all variables. Therefore, no convection and diffusion fluxes across the symmetry plane

Material Properties

For this study, the absorber is made of stainless steel with Specific Heat capacity 0.5 kJ/g ^oC and density 8 g/cm^3 [35] while the thermal conductivity varies with temperature according to $\lambda = 14.8 + 0.0153T_r$ [18]. The glass cover is taken as borosilicate Pyrex® whose properties were taken to be constant similar to those current receivers [11, 12, 15 and 18].

Air is taken as the annulus fluid with its density calculated by the Incompressible ideal gas law, the thermal conductivity varying according to equation (11) and the rest of the properties calculated using kinetic theory as given in ref. [33].

Syltherm 800 is used as the absorber tube heat transfer fluid used whose properties are input as functions of temperature according to polynomial functions equations (32-35) given by[21].

$$c_p = 0.001708T + 1.107798 \ (\mathrm{kJ/\ kg\ K}) \quad (32)$$

$$\lambda = -5.753496 \times 10^{-10} T^2 - 1.875266 \times 10^{-4} T + 1.9002 \times 10^{-1} \ (\mathrm{W/m^{-1}K}) \quad (33)$$

$$\rho = -4.153495 \times 10^{-1} T + 1.105702 \times 10^3 \ (\mathrm{kg\ m^{-3}}) \quad (34)$$

$$\mu = 6.672 \times 10^{-7} T^4 - 1.566 \times 10^{-3} T^3 + 1.388 T^2 - 5.541 \times 10^2 T + 8.487 \times 10^4 \ (\mu \mathrm{Pa\ s}) \quad (35)$$

Geometric parameters

A receiver with dimensions similar to those of the current SEGS-2 plants Dudley [11] was used in this study. Receiver dimensions are given in Table 1.

Table 1: Geometrical parameters

	Validation simulations	Base case
Receiver inner diameter(cm)	11.5	11.5
Absorber inner diameter (cm)	6.6	6.6
Absorber thickness (cm)	0.2	0.2
Receiver length (m)	7.8	4
Concentration ratio	71	71
Optical Efficiency (%)	73.2	73.2

Five different cases of the finned receiver were compared against the base case. Fin thickness is kept constant in all cases the same as the absorber thickness i.e. Case A 0.2 cm x 0.2 cm, Case B 0.6 cm x 0.2 cm, Case C 1.0 cm x 0.2 cm, Case D 1.4 cm x 0.2 cm and case E 1.8 cm x 0.2 cm. Case F considered a larger non-finned tube of absorber inner diameter 7.7cm and receiver inner diameter 13.5cm. Only the lower fin was varied since it is the one deemed to influence receiver performance.

SOLUTION PROCEDURE

The numerical solution of the governing equations was implemented in a commercial three dimensional package ANSYS® 13.0. The geometry built in ANSYS Design Modeler and the grid in ANSYS meshing. The mesh is refined with a fine mesh at the absorber annulus interface and at glass ambient interface as well as along the receiver's axial direction as shown in Figure 5. The solution is obtained in ANSYS FLUENT which uses a Finite Volume method for solving the governing continuity, momentum, energy and k-ε model equations. The computational domain was discretized using hexahedral and quadrilateral elements. Second order upwind scheme was employed for integrating the governing equations together with the boundary conditions over the computational domain and SIMPLE algorithm was used for coupling pressure and velocity. Radiation heat transfer in the annulus is modelled using the discrete ordinates model with air taken as a radiatively non-participating medium. Convergence was obtained with scaled residuals of mass, momentum, turbulent kinetic energy (k) and turbulence dissipation rate (ε) less than 10^{-4} while the energy residuals were less than 10^{-6} and when monitors of the convergence history of the absorber outlet temperature and glass temperature have flattened for more than 200 successive iterations.

Mesh independence studies for several refinements of the mesh were carried out with the receiver heat losses and heat gain as monitored quantities

$$\left|\frac{q_u^{\,i} - q_u^{\,i+1}}{q_u^{\,i+1}}\right| \le 0.01 \text{ and } \left|\frac{q_l^{\,i} - q_l^{\,i+1}}{q_l^{\,i+1}}\right| \le 0.01$$ Where i is the value before mesh refinement and i+1 is the value after mesh refinement.

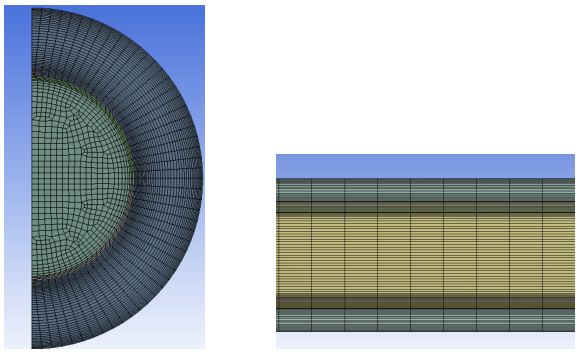

Figure 5 Mesh used in the study: Radial and axial directions

RESULTS AND DISCUSSION

The Numerical model was validated using the test results of Dudley [11] for heat gain and test results from Burkholder and Kutscher [18] for heat losses. Moreover, heat transfer was validated using Nusselt Number and fluid flow by friction factor. Petukhov second equation and Gnielinski correlations [34] were used for Nusselt number comparisons whereas Petukhov's first equation (29) was used for pressure drop validation.

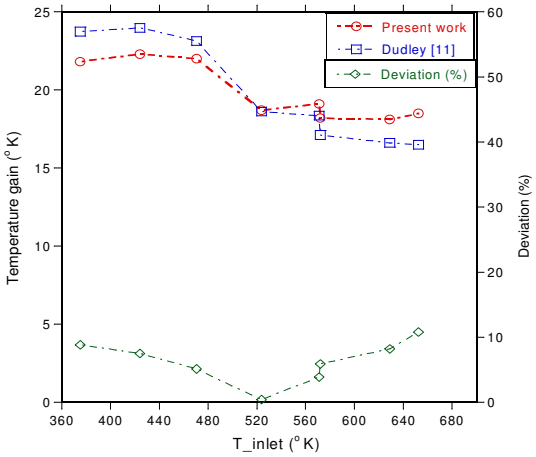

Figure 6 Validation of temperature gain

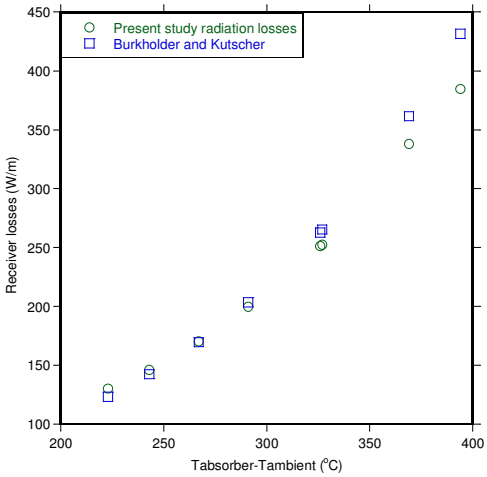

Figure 7 Validation of receiver heat losses

Temperature gain results were within less than 11% of experimental results obtained by Dudely [11] as shown in Figure 6. The correlation obtained by Burkholder and Kutscher [18] which relates heat losses to the difference between absorber temperature and ambient temperature was used to validate heat losses. The present study correlates well with the experimental data as shown in Figure 7 when only radiation losses are considered.

Nusselt number and friction factor also compare well with correlation data. Nusselt number was within less than 8% of both Petukhov's second equation and Gnielinski correlations as shown in Figure 8.

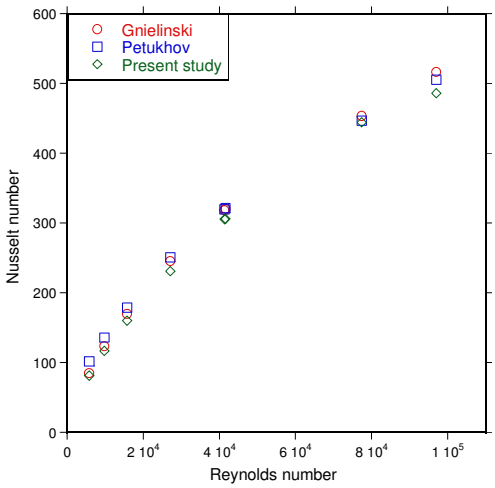

Figure 8 Validation of Nusselt number

Effect of external fins on pressure drop and heat transfer coefficient

External fin dimensions have no or negligible effect on the pressure drop and heat transfer characteristics for the same diameter of the absorber tube. When compared with the a non-finned absorber of diameter equal to finned absorber diameter plus the fin height there is some pressure drop penalty. As would be expected an increase in the flow rate or Reynolds number increases both the pressure drop and Nusselt number. Figure 9 shows the effect of external fins on Nusselt number. For a larger tube, the Nusselt number increases as a result of increased diameter of the tube and not as a result of increased heat transfer coefficient.

Effect of external fins on glass temperature and maximum absorber temperature

Figure 10 shows that as the height of the external fins increases the glass temperature also increases. Addition of external fins on the absorber implies that some heat must be transferred from the fin to the absorber by conduction while some of it is radiated to the space between the absorber and the glass cover. This transfer of heat is constrained by the fact that there is a limit on the amount of heat that can be transferred by the heat transfer fluid determined by the flow rate and the amount that can be radiated determined the absorber wall selective coating emissivity. This will affect the maximum temperature in the absorber tube and glass temperature as fin height increases. For all cases the average glass temperature remains within the normal operating range less than 100°C [15].

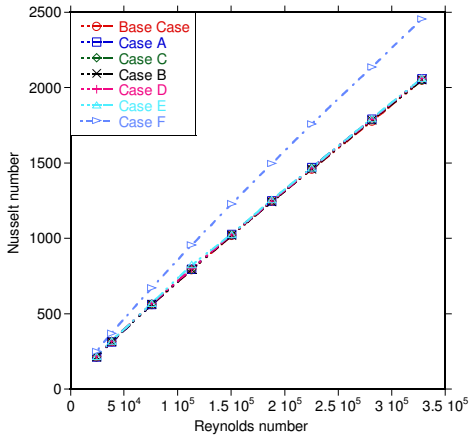

Figure 9 Variation of Nusselt number with Reynolds number

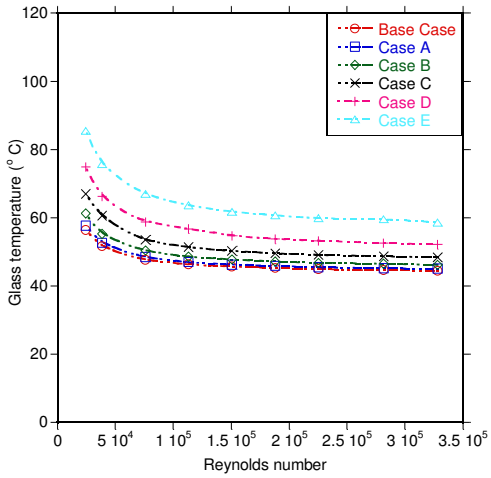

Figure 10 Variation of receiver glass temperature

Glass temperature reduces as the heat transfer fluid flow rate increase. As the fin height increases the absorber maximum temperature also increases. It will approach the maximum operation temperature of stainless steel under continuous operation about 1143°K [35] as the inlet temperature and concentration ratio increase.

Table 2 Effect of concentration ratio and inlet temperature on maximum wall temperatures

CR	T_{inlet} (° K)	Mass flow rate (kg/s)	$T_{ri,\,max}$ (°K)	$T_{ro,max}$ (°K)	T_{abs_ave} (°K)
80	650	7.84	688.16	795.97	664.58
90	650	7.84	692.70	812.73	666.38
100	650	7.84	697.39	829.91	668.18
80	700	7.84	742.09	844.11	716.39
90	700	7.84	747.67	861.81	718.51
100	700	7.84	753.34	879.66	720.65

For all cases considered the maximum absorber temperature is lower than the maximum working temperature and the melting point of stainless steel 1673°K [35]. As the concentration ratio and inlet temperature increase both glass

temperature and absorber maximum temperature are expected to increase. Table 2 shows some of the data for the effect of increasing inlet temperature and concentration ratio on the absorber inner and outer wall temperatures (T_{ri} and T_{ro}).

Effect of External Fins on Heat Gain and Efficiency

The heat gained by the working fluid and collector efficiency are observed to increase as the Reynolds numbers increases and then becoming nearly constant at Reynolds numbers of the order 7.5 x10^4 for both finned and non-finned absorber tubes. At low Reynolds numbers the efficiency increase slightly by about 3% and then becomes nearly constant as the Reynolds numbers increase as shown in Figure 11. This is because heat gained by the heat transfer fluid no longer increases significantly as the Reynolds number increases. As fin height increases the efficiency continually increases.

For the current flow rates used in the SEGS-2 plants the collector efficiency increases by about 11.6 % from 45% to 56.6% when a finned absorber tube is compared with same size non- finned tube and by 13.6% when a finned tube is compared with a larger non-finned tube for a fin of height 1.8 cm by thickness 0.2 cm. The larger absorber tube gives a low efficiency since the concentration ratio is slightly reduced.

Effect of external fins on heat losses

Figure 12 shows that as the fin height increases the receiver heat losses also increase. The increase is more pronounced at low Reynolds numbers. At higher Reynolds numbers heat transfer coefficients are higher and more heat is carried by the heat transfer fluid. At lower values of fin height the increase in losses is smaller and becomes larger as the fin height increases since most of the heat will not be conducted to the absorber tube. For smaller fin heights the heat losses are lower than for a larger non-finned absorber tube. The larger non-finned tube has a large heat loss area.

Even though the external fins increase efficiency of the receiver it should be noted that there are limiting factors to their use. These include: the temperature of the absorber tube outer wall currently limited to about 400°C to avoid degradation of the absorber tube's selective coating; the temperature of the absorber tube inner wall to avoid degradation of the heat transfer fluid whose current operation temperatures are limited to 400°C [4].

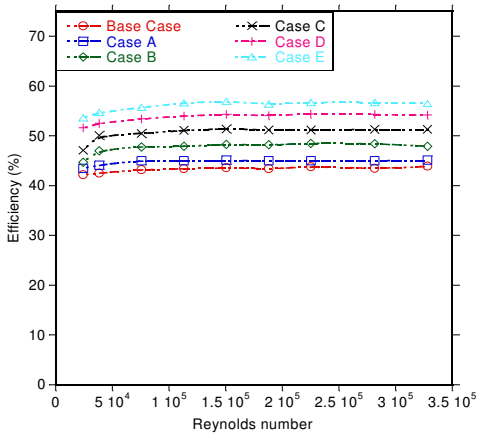

Figure 11 Variation of collector efficiency

Therefore, fin dimensions should be selected such that they improve performance without compromising the life of the receiver.

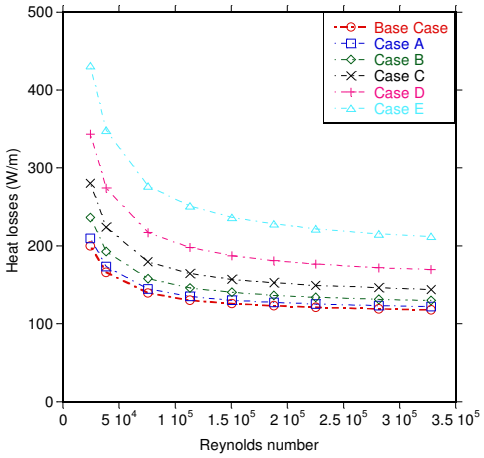

Figure 12 Variation of heat losses with fin dimensions and Reynolds number

From the study, with the assumed constant heat flux (DNI 933W/m^2) the absorber wall inside temperature remains lower than 673 °K for all fin heights and concentration ratios 71, 80, 90 and 100 provided the inlet temperature does not exceed 600°K and heat transfer fluid mass flow rates are kept higher than 6.09 kg/s. For flow rates above 6.09 kg/s and inlet temperature less than 550°K the maximum outer absorber temperature is kept within less than 673° K at a concentration ratio of 71.

For a fin of dimensions 1 cm x 0.2 cm the efficiency increases by 6% and 8% when compared to the two non-finned cases respectively for an inlet temperature of 523°K. The smaller tube gives an additional pressure drop of 370.65Pa/m (3.27W/m additional pumping power) when compared with the larger non-finned tube and an increase in heat gain of 444.2 W/m

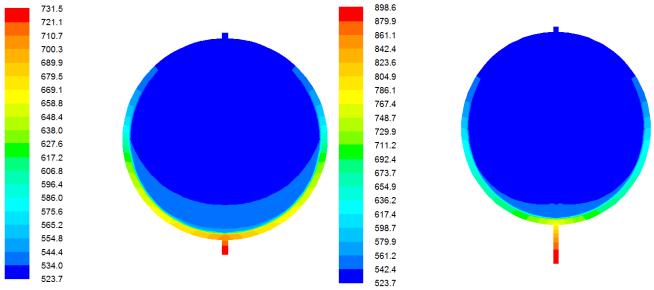

(a) 0.5 cm x 0.2 cm fin (b) 1.4 cm x 0.2 cm fin

Figure 13 Contours of temperature at absorber outlet at Reynolds number 2.44x10^4, C_R=71, DNI =933W/m^2 for 0.5 cm x 0.2 cm and 1.4 cm x 0.2 cm finned absorber tubes

As the concentration ratio, inlet temperatures and fin height increase the maximum temperature inside and outside the absorber tube will increase and exceed 673°K. The maximum temperature is concentrated on the lower fin as shown in the contours of temperature in Figures 13 and 14. Using higher flow rates is one way of decreasing the maximum absorber wall temperatures. Combining the outer fins with

inner fins is likely to significantly reduce the maximum outer absorber maximum inner absorber temperature.

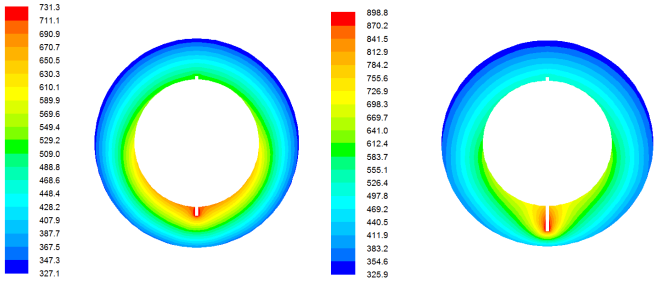

(a) 0.5 cm x 0.2 cm fin (b) 1.4 cm x 0.2 cm fin

Figure 14 Contours of annulus temperature at a Reynolds number 2.44×10^4, C_R=71, DNI =933W/m^2 for 0.5 cm x 0.2 cm and 1.4 cm x 0.2 cm finned absorber

CONCLUSION

A numerical model to evaluate the performance of an externally finned parabolic trough receiver was developed. From the study it can be concluded that including external fins on the absorber tube improves performance of receiver. The longer the fin, the more is the heat gain, the higher the efficiency but also the higher the heat losses, glass temperature and absorber tube maximum temperature.

For concentration ratios between 71 –100 and flow rates higher than 6.09kg/s the maximum absorber inner wall temperature will exceed 673^{o}K when inlet temperatures greater than 600^o K are used. The maximum absorber outer wall temperature exceeds 673^{o}K when inlet temperatures higher than 550^{o}K are used.

A combination of external fins and internal fins can be studied to evaluate the effect of different fin configurations on the performance and the possible reduction of absorber tube maximum temperatures.

ACKNOWLEDGEMENT

The authors acknowledge the support received from Department of Mechanical and Aeronautical Engineering, University of Pretoria, Pretoria, South Africa

NOMENCLATURE

A	[m^2]	Area
a	[m]	Collector aperture width
c_p	[Jkg^{-1} K^{-1}]	Specific heat capacity
C_R	[-]	Concentration ratio
d_r	[m]	Absorber tube diameter
D	[m]	Hydraulic diameter
DNI	[W/m^2]	Direct Normal Irradiation
f	[-]	Friction factor
f_p	[m]	Focal length
g	[m/s^2]	Acceleration due to gravity
h	[W/m^{2}K]	heat transfer coefficient
I_b	[W/m^2]	Direct solar radiation
k	[m^2/s^2]	Turbulent kinetic energy
L	[m]	Reciever length
$\dot{m}_f$	[kg/s]	Fluid mass flow rate
Nu	[-]	Nusselt number
P	[Pa]	Presure
Pr	[-]	Prandtl number
q_u	[W]	Heat gain
Q_{loss}	[W]	Heat loss
q''	[W/m^2]	Heat flux
Ra	[-]	Raleigh number
Re	[-]	Reynolds number
R_s	[kJkg^{-1} K^{-1}]	Specific gas constant
t	[cm]	Thickness
T	[^{o} K]	Temperature
U	[m/s]	Mean velocity
u, v	[m/s]	Velocity components
$\dot{V}$	[m^3/s]	Volume flow rate
W	[m]	Flat receiver width
x, r	[m]	Spatial coordinates

Greek letters

Φ	[Wm^{-2}K^{-4}]	Stefan Boltzman Constant
β	[^{o}C^{-1}]	Coefficient of thermal expansion
ε	[m^2/s^3]	Turbulent dissipation rate
ξ	[-]	Emissivity
η	[%]	Efficiency
η_0	[%]	Optical efficiency
ρ	[kg/m^3]	Density
ρ_r	[m]	Collector rim radius
τ_g	[-]	Glass cover transmissivity
τ_w	[N/m^2]	Wall shear stress
λ	[Wm^{-1} K^{-1}]	Thermal conductivity
φ_r	[degrees]	Collector rim angle
μ	[Pa s]	Viscosity
ν	[m^2/s]	Kinematic viscosity
χ	[m]	Molecular mean free path

Subscripts

Amb	Ambient state
eff	Effective value
ref	Reference value
gi	Glass inner side
go	Glass outer side
in	Inlet
L	Length
out	Outlet
p	Near wall node
r	Absorber
ri	Absorber inner
ro	Absorber outer
sky	Sky
t	Turbulent

Super scripts

-	Time averaged value

REFERENCES

[1] IEA, World Energy Outlook 2010 Executive summary, International Energy Agency Publications, 2010

[2] Kalogirou S., Solar Energy Engineering: Processes and Systems, 1st Ed., Elsevier, Oxford U.K. 2009

[3] DESERTEC., Clean power from deserts – the DESERTEC concept for Energy, Water and Climate security the White book 4th Edition 2009.

[4] Prince H., Lupfert E., Kearney D., Zarza E., Cohen G., Gee R., Mahoney R., Advances in Parabolic Trough Solar Power Technology, *ASME Journal of Solar Energy Engineering*, Vol.124, 2002, pp.109-125
[5] IEA, Technology Roadmap, Concentrating Solar Power, *International Energy Agency Publication,* 2010
[6] Concentrating solar power outlook 2009, *a Greenpeace International, SolarPACES and ESTELA publication*
[7] Prince H., Kearney D., Reducing the cost of energy from parabolic trough solar power plants, *Proceedings of the International solar energy conference*, Hawaii Island, March 2003
[8] Tyagi S.K., Shengwei W., Singhal M.K., Kaushik S.C., Park S. R., Exergy Analysis and Parametric Study of Concentrating type Solar Collectors, *International Journal of Thermal Sciences*, Vol. 46, 2007, pp.1304-1310
[9] Kalogirou S., Parabolic trough collector system for low temperature steam generation: Design and Performance Characteristics, *Journal of Applied Energy*, Vol.55, 1996, pp.1-19
[10] Kalogirou S., Lloyd S., Ward J., Modeling, optimization and performance evaluation of a parabolic trough solar collector steam generation system, *Journal of Solar Energy*, Vol.60, No. 1, 1997, pp.49-59
[11] Dudley V.E., Kolb G.J., Mahoney A.R., Mancini T.R., Matthews C.W., Sloan M., Kearney D., Test results: SEGS LS-2 Solar collector, *SANDIA REPORT*, 1994, SAND94-1884
[12] Dudley V.E., Evans L.R., Matthews C.W., Test Results: Industrial Solar Technology Parabolic Trough Solar Collector, *SANDIA REPORT,* 1995, SAND94-1117
[13] Odeh S.D. and Morrison G.L., Optimization of parabolic trough solar collector system, *International Journal of Energy Research,* Vol.30, 2006, pp.259-271
[14] Liu Q., Wang Y., Gao Z., Sui J., Jin H., and Li H., Experimental investigation on parabolic trough solar collector for thermal power generation, *Journal of Science China Technological Sciences*, Vol.53, No.1, 2010, pp.52-56
[15] Prince H., Forristall R., Wendelin T., Lewandowski A., Moss T., Gummo C., Field survey of Parabolic Trough receiver thermal performance. *In conference proceedings: ASME International Solar Energy Conference, ISEC2006,* 2006, *Denver*, Colorado, USA
[16] Lüpfert E., Pfänder M., Schiricke B., Eck M., Determination of temperature distribution on parabolic trough receivers, *SolarPACES2006*, 2006, A1-S6
[17] Lüpfert E., Riffelmann K.J., Prince H., Burkholder F., Moss T., Experimental analysis of overall thermal properties of parabolic trough receivers, *Journal of Solar Energy Engineering,* Vol.130, 2008, pp.12007-12011
[18] Burkholder F. and Kutscher C., Heat-loss testing of Solel's UVAC3 parabolic trough receiver, *National Renewable Energy Laboratory Technical Report*, 2008, NREL/TP-550-42394, U.S. Department of Energy
[19] Burkholder F. and Kutscher C., Heat-loss testing of Scott's 2008 parabolic trough receiver, *National Renewable Energy Laboratory Technical Report,* 2009, NREL/TP-550-45633, U.S. Department of Energy
[20] Foristall R., Heat transfer analysis and modelling of a parabolic trough solar receiver implemented in Engineering Equation Solver, *National Renewable Energy Laboratory Technical Report*, 2003, U.S Department of Energy, NREL/TP-550-34169
[21] Ya-Ling He, Jie Xiao, Ze-Dong Cheng, Yu-Bing Tao 2011, A MCRT and FVM coupled simulation method for energy conversion process in parabolic trough solar collector, *Journal of Renewable Energy,* Vol.36, pp. 976-985
[22] Hegazy A.S., Thermal performance of a parabolic trough collector with a longitudinal externally finned absorber, *Journal of Heat and Mass Transfer*, Vol.31, 1995, pp. 5-103
[23] Reddy K. S., Ravi Kumar K., and Satyanarayana G.V., Numerical Investigation of Energy Efficient Receiver for Solar Parabolic Trough Concentrator, *Journal of Heat Transfer Engineering,* Vol.29, No.11, 2008, pp. 961-972.
[24] Ravi Kumar R., Reddy K.S, Thermal analysis of solar parabolic trough with porous disc receiver, *Journal of Applied Energy*, Vol.86, 2009, pp.1804-1812
[25] Munoz J., Abanades A., Analysis of internally helically finned tubes for parabolic trough design by CFD tool, *Journal of Applied Energy*, Vol.88, No.11, 2011, pp.4139-4149
[26] John A. Duffie, William A. Beckman, Solar engineering of thermal processes, 3rd Ed. 2006, John Wiley and Sons Inc. Hoboken, New Jersey
[27] Mathew Roesle, Volkan Coskun, Aldo Steinfeld, Numerical analysis of heat loss from a parabolic trough absorber tube with active vacuum system, *ASME Journal of Solar Energy Engineering* Vol.133, 2011, 031015-1
[28] Joseph A. Potkay, Gordon Randall Lambertus, Richard D. Sacks, A low-pressure and temperature-programmable micro gas chromatography column, *Journal of Micro electro-mechanical systems,* Vol.16, No.5, 2007
[29] Garcia-Valladares O., Valazquez N., Numerical simulation of parabolic trough solar collector-Improvement using counter flow concentric heat exchangers, *International Journal of Heat and Mass Transfers* Vol.52, 2009, pp.597-609
[30] Bejan A., Convection heat transfer 3rd Ed., 2004, John Wiley & sons, Inc, Hooken, New Jersey
[31] Pritam D., Debajit S., Snehamoy M., Turbulent fluid flow analysis in a circular axisymmetric duct having closed inlet with side jet flow, *International journal of Engineering Science and Technology*, Vol.3, No.1, 2011, pp.5578-5592
[32] Henk Kaarle Versteeg, Weeratunge Malalasekera, An introduction to Computational Fluid Dynamics: the finite volume method 2nd Ed., 2007, Pearson Education Ltd
[33] ANSYS FLUENT, Theory guide, Release 13.0, 2010. ANSYS, Inc. Southpointe 275 Technology Drive, Canonsburg, PA15317
[34] Yunus A. Cengel, Heat transfer; A Practical Approach 2nd Ed., 2002, McGraw-Hill Companies, Inc. New York
[35] Limatherm Sp.zo.o., Technical information for stainless steel DIN 1.4541 (V2A), AISI 321 specification, 2004. available at www.limatherm.com last accessed 25th August 2011